Turkish Journal of Chemistry
http://journals.tubitak.gov.tr/chem/
Research Article

Turk J Chem
(2014) 38: 99 – 108

doi:10.3906/kim-1212-39

A combined first principles TDDFT and experimental study on the UV-Vis spectra properties of M(p-nitrophenyl azo resorcinol)$_3$ complexes (M: Fe, Cr)

Tuğba TÜĞSÜZ ARİFİOĞLU*, Melis EFEÇINAR, Nuray ŞATIROĞLU
Department of Chemistry, Hacettepe University, Beytepe, Ankara, Turkey

Received: 14.12.2012 • **Accepted:** 09.07.2013 • **Published Online:** 16.12.2013 • **Printed:** 20.01.2014

Abstract: UV-Vis absorption data of p-nitrophenyl azo resorcinol (Magneson I) and its 2 Fe(III) and Cr(III) complexes were investigated both experimentally and theoretically. The geometries were optimized at BP86/TZVP level. The most stable spin states were computed as doublet and quartet for Fe(magneson)$_3$ and Cr(magneson)$_3$ complexes, respectively. Time-dependent density functional theory (TDDFT) was employed to explore the absorption spectra properties, whereas the solvent effects were taken into account using the polarizable continuum model (PCM). The M06, B3LYP, and PBE0 hybrid functionals together with TZVP/LANL2TZ basis sets were used for comparing the results with experimental data. The theoretical analysis of electronic structure and molecular orbitals demonstrated that the low-lying absorption bands in the UV-Vis spectra are mainly $\pi \rightarrow$ d ligand-to-metal charge transfer (LMCT) transition and $\pi \rightarrow \pi$ ligand-to-ligand charge transfer (LLCT) transition for Fe(magneson)$_3$, and, in addition to that of LMCT and LLCT, d $\rightarrow \pi$ metal-to-ligand charge transfer (MLCT) transition for Cr(magneson)$_3$ complexes. The good agreement between the experimental and TDDFT calculation, especially M06 and B3LYP absorption spectra of the metal Magneson I complexes, allowed us to provide a detailed estimation of the main spectral features of ferric and chromic complexes.

Key words: p-Nitrophenyl azo resorcinol, Magneson I, iron(III), chromium(III), DFT, TDDFT

1. Introduction

Metal complexes and metal complexed azo dyes are used widely in the textile industry,[1] photoelectronic applications,[2] optical devices,[3] organic light-emitting diodes (OLEDs),[4] chemosensors, and biotechnology probes.[5]

Azo dyes are synthetic colors containing an azo group (–N=N–) as part of the structure. The azo groups are generally connected to benzene and naphthalene rings. Occasionally, they are also attached to aromatic heterocycles or to enolizable aliphatic groups.[6a] These side groups around the azo bond help to stabilize the N=N group by making it part of an extended delocalized system. This also has the effect of making many azo compounds colored, as delocalized or conjugated systems often absorb visible frequencies.[6b] The azo group has not been observed to coordinate with a metallic atom to form a stable complex unless the metal can be held by chelation within the dye molecule. Azo dyes must therefore possess a hydroxyl, amino, or other group in opposition to the azo group to enable the metal atom to be implicated in a chelate ring. Further, only one nitrogen atom of the azo group enters into coordination; copper complexes have been assigned structures in which both the nitrogen atoms of an azo group coordinate with the metallic atoms, but such complexes are to

*Correspondence: ttugsuz@hacettepe.edu.tr

be regarded as resonance hybrids of azo and quinonehydrozone structures.[7] Azo violet, 4-(p-nitrophenyl azo resorcinol) (Magneson I), is an azo dye. Although Magneson I can be interacted with metals, forming different colors, it has been much less reported.[8] This is a first principles study to explore the complexation behavior of Fe(III) and Cr(III) with Magneson I.

The spectroscopic, photochemical, and photophysical behavior of transition metal azo dye complexes can be explained by the use of quantum chemical studies. Modern density functional theory (DFT) calculations have proved highly successful at predicting the structures and electronic properties of transition metal complexes. In addition, time-dependent DFT (TDDFT)[9] calculations allow quantum chemists to probe the nature of the excited states of complexes and facilitate a better understanding of observed electronic absorption spectra.[10]

In this first principles study, we take a closer look at the geometric and electronic structures of the Fe and Cr complexes of Magneson I with the results obtained from the DFT calculations performed to understand the interaction that is going on around the central metal ion and specifically to get a better insight into its interaction with the Magneson I ligand. Another aim of this research is to provide a theoretical understanding of the spectroscopic properties of the 1:3 complexes of Fe(III) and Cr(III) with Magneson I. To achieve this goal, theoretical electronic spectra of the most stable complex structures are compared to the experimental data recorded in water solution (at pH 7). Overall, we are interested in the design of new ligands and complexes for the development of colored complexes for determining Fe(III) and Cr(III).

2. Experimental

2.1. Reagents

All solutions were prepared with deionized water (18.1 MΩ cm) obtained from a Barnstead Nanopure Diamond purification system. All chemicals used were of analytical reagent grade. Standard solutions (1000 μg mL^{-1}) of Fe(III) and Cr(III) were prepared by dissolving appropriate amounts of the respective nitrates (Merck, Darmstadt, Germany) in deionized water. A 0.2% Magneson I solution obtained from Sigma-Aldrich was prepared in ethanol (Merck). A buffer solution of pH 7 was prepared by using acetic acid (Merck), sodium acetate (Merck), and sodium hydroxide (Merck) at appropriate concentrations. Laboratory glassware was kept overnight in 10% nitric acid solution. Before use, the glassware was rinsed with deionized water and dried in a dust-free environment.

2.2. Instrumentation

A Shimadzu UV-Vis spectrophotometer (Model mini–1240, Kyoto, Japan) was used for spectrophotometric measurements (1.0 cm quartz cell) of the metal–Magneson I complex. The measurements were obtained between 400 and 800 nm. A Fisher Scientific Accumet model 15 pH meter was used to measure pH values.

2.3. Procedure

Aliquots of 12.5 mL of a solution containing iron(III) or chromium(III) ions, 1 mL of acetate buffer solution with NaOH (pH 7), and 0.5 mL of 0.2% Magneson I solution were placed in a graduated tube. The mixture was shaken and the resultant solution was transferred into a quartz cell for UV-Vis measurement.

3. Computation

All calculations were performed by DFT using the Gaussian 09 program.[11] The complexes were treated as an open-shell system using spin-unrestricted DFT wavefunctions. As the Fe(III) system has a 3d^5 configuration,

in its complex Fe(III) central atom can be in the low-spin (S = 1/2), intermediate-spin (S = 3/2), or high spin (S = 5/2, S = 3/2) state.[12] The electrons presented in the Cr(III) central metal ion have a $3d^3$ electronic configuration and the spin state of the central Cr(III) can be S = 1/2 or S = 3/2. It is important to note that the complex is low spin with S = 1/2, which is not usual for $3d^3$ chromium(III) complexes, generally known to have 3 spin-allowed transitions (high spin, S = 3/2) with the 3 electrons occupying 3 different degenerate orbitals.[13] Thus, DFT optimized calculations were carried out in different spin states with S = 1/2, 3/2, and 5/2 for Fe(III) and with S = 1/2 and 3/2 for Cr(III) complexes with Magneson I, respectively. The geometries of metal(III) Magneson I complexes were optimized in gas phase by using the nonhybrid UBP86 functional[14] together with the valence triple ζ quality with polarization function basis set, TZVP,[15] without any symmetry constraint. For the geometry-optimized structure of each species, the frequencies were calculated to ensure a transition state or saddle point structure was not obtained.

Molecular orbital energies of ground state complexes were taken from M06,[16] B3LYP,[17] and PBE0[18] hybrid functionals. The "Triple ζ" quality and polarization basis sets were employed for the C, H, N, and O atoms (TZVP) and the Fe and Cr (LANL2TZ(f)).[19] To obtain the vertical excitation energies of the low-lying singlet excited states of the complexes, TDDFT calculations using the M06, B3LYP, and PBE0 hybrid functionals in water were performed at the respective ground state geometries. LANL2TZ was again used for Fe and Cr, while for the C, H, N, and O atoms the TZVP basis set was used. Typically the 20 lowest singlet excited states of the open shell complexes were calculated for comparing with the experimental absorption spectra and examining each peak. Solvent effects (water) were introduced by the SCRF method, via the polarizable continuum model (PCM)[20] implemented in the GAUSSIAN 09 program, for both SCF energies and TDDFT calculations. The cavity for the solute molecule was built from a group of overlapping spheres. The universal forcefield (UFF) model, which places a sphere around each solute atom, was applied to build up the molecular cavity.

4. Results and discussion

4.1. Geometries

In order to neutralize the charge of the overall molecule, a metal-to-ligand mol ratio of 1:3 was adopted to the molecular design of both structures. The structural stability and energetic and electronic properties of Fe(magneson)$_3$ and Cr(magneson)$_3$ were investigated with BP86/TZVP level of theory. The most stable spin states were computed as doublet and quartet for Fe(magneson)$_3$ and Cr(magneson)$_3$ complexes, respectively. Thus, the S = 1/2 and S = 3/2 is in fact a ground state for these ferric and chromic complexes, respectively.

The optimized ground state structures of Fe(magneson)$_3$ and Cr(magneson)$_3$ complexes are shown in Figure 1. Selected bond lengths and angles for the optimized geometrical parameters of all complexes are reported in Table 1. The calculated M–N and M–O distances of ground state structures for Fe(magneson)$_3$ were 2.0 and 1.9 Å and for Cr(magneson)$_3$ were 2.1 and 2.0 Å, respectively. Moreover, these results are similar to the values of bond length ranges of complexes in most of the low spin ferric and chromium(III) complexes studies.[13a,21–23]

The angles between trans ligands were smaller than 180°. The N2–M–N3, N1–M–O2, and O1–M–O3 angles were for Fe(magneson)$_3$ complex 170.5°, 176.4°, and 174.3° and for Cr(magneson)$_3$ complex were 169.3°, 175.2°, and 177.4°, respectively. Moreover, the angles between the cis ligands were close to 90°. The N1–M–O1, N1–M–O3, and O1–M–O2 angles were for Fe(magneson)$_3$ complex 93.70°, 91.43°, and 89.63°, and

for Cr(magneson)$_3$ complex were 94.74°, 87.61°, and 89.85°, respectively. It was also observed that for the 3 equatorial M–O bonds, 2 were always the same in length (M–O1 and M–O3), while 1 was longer in length (M–O2). This can be attributed to the fact that at any point in time the structures maintained a distorted octahedral geometry.

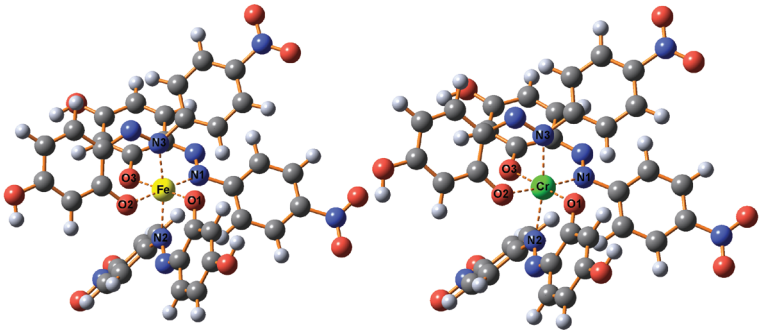

Figure 1. The optimized ground state structures for Fe(magneson)$_3$ and Cr(magneson)$_3$.

Table 1. Main optimized geometrical parameters of the Fe(magneson)$_3$ and Cr(magneson)$_3$ complexes in different spin state at the BP86/TZVP level.

	Fe(magneson)$_3$			Cr(magneson)$_3$	
Bond lengths (Å)	S = 1/2	S = 3/2	S = 5/2	S = 1/2	S = 3/2
M–N1	1.961	1.993	2.218	2.037	2.094
M– N2	2.004	2.279	2.205	2.055	2.099
M–N3	1.997	2.244	2.257	2.096	2.115
M–O1	1.908	1.914	1.972	1.914	1.951
M–O2	1.939	1.911	1.994	1.971	1.962
M–O3	1.894	1.914	1.985	1.895	1.954
Bond angles (°)					
∠ N1–M–N2	98.01	99.09	102.0	98.18	97.86
∠ N1–M–N3	81.49	95.14	91.76	92.61	92.76
∠ N2–M–N3	170.5	165.5	166.1	169.2	169.3
∠ N1–M–O1	93.70	91.47	94.24	95.15	94.74
∠ N1–M–O2	176.4	177.2	169.1	175.3	175.2
∠ N1–M–O3	91.43	89.43	82.27	88.62	87.61
∠ O1–M–O2	89.63	91.26	94.56	89.36	89.85
∠ O1–M–O3	174.3	177.5	176.4	175.9	177.4
∠ O1–M–N2	90.59	83.31	83.26	88.13	87.47
∠ O1–M–N3	90.28	93.36	93.82	91.76	92.63
Dihedral angles (°)					
∠ O3–M–N1–O1	177.6	177.7	179.2	178.4	178.8

4.2. Electronic spectra of the complexes

The computed absorption bands, dominant transitions, characters, and oscillator strengths together with experimental data of Fe(magneson)$_3$ and Cr(magneson)$_3$ complexes are given in Table 2. The calculated transition wavelengths from M06, B3LYP, and PBE0 of free Magneson I molecule are in good agreement with the experimental values. According to the experimental results, Magneson I has the most intense absorption

Table 2. Computed and experimental UV-Vis absorption bands, dominant transitions, and oscillator strengths of Fe(magneson)$_3$ and Cr(magneson)$_3$ complexes.

	M06		B3LYP		PBE0		Expt.	
	λ	ossc.	λ	ossc.	λ	ossc.	λ	Absorbance
Magneson	215 67–72 H → L + 4	0.0220	224 66–70 H – 1 → L + 2	0.0302	213 66–70 H – 1 → L + 2	0.0289	213	0.0073
	283 63–68 H – 4 → L	0.0211	299 66–69 H – 1 → L + 1	0.0393	279 66–69 H – 1 → L + 1	0.0316	300	0.0016
	326 64–68 H – 3 → L	0.0206	332 64–68 H – 3 → L	0.0193	317 64–68 H – 3 → L	0.0206		
	329 67–69 H → L + 1	0.0508	344 67–69 H → L + 1	0.1169	325 67–69 H → L + 1	0.0689		
	446 67–68 H → L	0.9083	459 67–68 H → L	0.8112	439 67–68 H → L	0.8951	450	0.0918
Fe(magneson)$_3$	506 204b–211b S – 3 → L + 3 MMCT/LMCT	0.0449	503 208a–210a S → L + 1 LLCT	0.0295	506 207b–208b S → L LLCT	0.0262		
	532 207b–209b S → L + 1 MMCT/LMCT	0.0130	534 208a–209a S → L LLCT	0.0255	516 208a–215a S → L + 6 LMCT	0.0027	534	0.0570
	543 206b–208b S – 1 → L LMCT	0.0104	549 207b–208b S → L LLCT	0.0156	534 193a–216a S – 15 → L + 7 MMCT/LMCT	0.0006		
	659 208a–211a LLCT S → L + 2	0.0008	679 208a–211a LLCT S → L + 2	0.0008	689 208a–211a LLCT S → L + 2	0.0003	669	0.0110
	666 206a–209a S – 2 → L LLCT	0.0004	690 206a–209a S – 2 → L LLCT	0.0007	699 206a–209a S – 2 → L LLCT	0.0003		
	679 207b–208b S → L MMCT/LMCT	0.0005						
Cr(magneson)$_3$	497 208a–210a S → L + 1 MLCT	0.0486	521 208a–210a S → L + 1 LLCT	0.028	479 208a–210a S → L + 1 LL CT	0.0419	532	0.0320
	537 208a–209a S → L MLCT	0.0083	553 208a–209a S → L LLCT	0.047	529 208a–209a S → L LLCT	0.0159	570	0.0420
	576 201a–215a S – 7 → L + 6 MMC/LMCT	0.0007						
	647 207a–215a S – 1 → L + 6 LMCT	0.0005					640	0.0230
	684 204b–206b S – 1 → L LLCT	0.0006	697 204b–208b S – 1 → L + 2 LLCT	0.0007	703 204b–208b S – 1 → L + 2 LLCT	0.0004	672	0.0300

maximum at 450 nm. The computed results also matched the experimental ones. In the computation, M06 functional has little difference (3 nm) while the other B3LYP and PBE0 functionals have 9 and 11 nm differences from the maximum absorption value.

In the Fe(magneson)$_3$ complex, the bands with large oscillator strength (0.0449, 0.0295, and 0.0262) were obtained at 506, 503, and 506 nm with M06, B3LYP, and PBE0, respectively. The 532, 534, and 516/534 nm absorption bands with 0.0130, 0.0255, and 0.0027/0.0006 oscillator strengths taken from M06, B3LYP, and PBE0, respectively, could be readily associated with the experimental low-lying absorption band (534 nm). These absorptions were due to dominant contributions of the following orbital transitions: S $\rightarrow$ L + 1, S $\rightarrow$ L, and S $\rightarrow$ L + 6/S – 15 $\rightarrow$ L + 7 for M06, B3LYP, and PBE0, respectively, where "S" and "L" denote the "highest singly occupied molecular orbital" and the "lowest unoccupied molecular orbital", respectively.

According to molecular orbital analysis (Table 3), with the exception of β–spin S and S – 3 (in M06) and α–spin S – 15 (in PBE0) of Fe(magneson)$_3$ complex and α–spin S and S – 7 (in M06) of Cr(magneson)$_3$ complex, which are an admixture of d orbital of central metal(III) and π bonding orbital of ligand, all these molecular orbitals involved in the corresponding transitions are ligand π bonding orbitals. Thus, for the Fe(magneson)$_3$ complex, the 506, 532, and 679 nm bands from M06 and the 534 nm band from PBE0, and, for the Cr(III) complex, the 576 nm band from M06 can be mainly ascribed to metal-to-metal charge transfer (MMCT) transition. Because of the considerable contributions from Lapporte-forbidden d–d transition, these absorption bands, in a sense, can also be regarded qualitatively as a d–d ligand-field band in nature, admixed with ligand-to-metal charge transfer (LMCT) transition, and this assignment is consistent with the facts for absorption and consistent with the ligand-field theory level expectation.[13a] Because of the π orbital character of ligand C and O atoms for α–spin S and the π^* orbital character of ligand N atoms for α–spin L, the transitions from B3LYP computation at 534 nm and 553 nm for Fe(magneson)$_3$ and Cr(magneson)$_3$ complexes, respectively, can be reasonably ascribed to ligand-to-ligand charge transfer (LLCT) transition. The 537 nm computed from M06 for Cr(magneson)$_3$ complex has metal-to-ligand charge transfer (MLCT) transition because its α–spin S has the d orbital character of chromium(III) and α–spin L has the π^* orbital character of N atoms of Magneson I ligand. The α–spin S of Fe(III) computed from PBE0 is composed of Magneson I at 38%, whereas the α–spin L + 6 consists of 51% d(Fe). Thus, the absorption band at 516 nm can be described as LMCT transition.

We also predicted other absorption bands for Fe(magneson)$_3$ complex at 543 and 549 nm with M06 and B3LYP, respectively. Furthermore, weak absorption bands in the 650–700 nm range with smaller oscillator strengths than for those mentioned above were also obtained from considered functionals to compare with the experimental result at 669 nm. The 15–30 nm shifts in wavelength are usual for TD–DFT-based excitation energy calculations.[13a]

Considering Table 2, we attribute the 497, 521, and 479 nm absorptions to MLCT, LLCT, and LLCT, which are consistent with the experimental value (532 nm) for Cr(magneson)$_3$ complex. The 537, 553, and 529 nm bands obtained from M06, B3LYP, and PBE0, respectively, show a similar transition character (S $\rightarrow$ L). Although the B3LYP absorption band at 553 nm matches the experimental absorption band at 570 nm, the additional band at 576 nm attributed to LMCT obtained from M06 is the closest one, with 6 nm differences. Furthermore, the experimental absorption band at 640 nm was obtained by only M06 functional at 647 nm with small oscillator strength (0.0005). The lower energy transitions at 684, 697, and 703 nm originate mainly from the S – 1 to L (M06) and to L + 2 (B3LYP and PBE0) transitions and the M06 band can be readily associated with the experimental absorption band with only 12 nm difference.

Table 3. Selected molecular orbital contributions of Fe(magneson)$_3$ and Cr(magneson)$_3$.

Fe(magneson)$_3$				Cr(magneson)$_3$			
Orbital number		Contribution (%)		Orbital number		Contribution (%)	
alpha	beta	alpha	beta	alpha	beta	alpha	beta
M06/TZVP + LANL2TZf				M06/TZVP + LANL2TZf			
211	211	N p = 0.27 O p = 0.24	Fe d = 0.43	215		Cr d = 0.40	
210	210	N p = 0.11	N p = 0.26 O p = 0.25	210	210	N p = 0.24 O p = 0.20	Cr d = 0.12 N p = 0.15 O p = 0.22
209	209	N p = 0.13	Fe d = 0.12	209	209	N p = 0.12	Cr d = 0.14 N p = 0.13
	208		Fe d = 0.15		206		N p = 0.14
	207		Fe d = 0.22 C p = 0.22	208		Cr d = 0.15	
208		C p = 0.11		207		C p = 0.25	
207		C p = 0.13 O p = 0.10		205	205	C p = 0.26	C p = 0.33 N p = 0.12
206	206	C p = 0.31 N p = 0.11 O p = 0.10	C p = 0.14	204	204	C p = 0.20	C p = 0.32 N p = 0.12
205	205	C p = 0.38	Fe d = 0.38	201	201	Cr d = 0.24 N p = 0.10	C p = 0.25
204	204	C p = 0.28	Fe d = 0.13 C p = 0.11				
B3LYP /TZVP + LANL2TZf				B3LYP /TZVP + LANL2TZf			
211	211	N p = 0.27 O p = 0.28	Fe d = 0.47	210	210	N p = 0.27 O p = 0.25	N p = 0.37
210	210	N p = 0.13 O p = 0.22	N p = 0.27 O p = 0.28	209	209	N p = 0.11	N p = 0.14 O p = 0.20
209	209	N p = 0.12	N p = 0.08		208		N p = 0.09
	208		N p = 0.11		206		N p = 0.13
208		C p = 0.26 O p = 0.10		208		C p = 0.09	
207	207	C p = 0.27 O p = 0.13	O p = 0.11 C p = 0.11	207		C p = 0.22 O p = 0.10	
206	206	C p = 0.31 O p = 0.11 N p = 0.11	C p = 0.10	204	204	C p = 0.42	C p = 0.32 N p = 0.12
PBE0 /TZVP + LANL2TZf				PBE0 /TZVP+LANL2TZf			
216		Fe d = 0.60		210	210	N p = 0.20	N p = 0.24
215		Fe d = 0.51		209	209	N p = 0.12	N p = 0.14 O p = 0.20
211	211	N p = 0.27 O p = 0.25	Fe d = 0.28		208		N p = 0.10
209	209	N p = 0.13	N p = 0.10		207		N p = 0.27
	208		N p = 0.13		206		N p = 0.14
208		C p = 0.28 O p = 0.10		208		C p = 0.10	
207	207	C p = 0.28 O p = 0.13	C p = 0.10 O p = 0.11	207		C p = 0.22	
206	206	C p = 0.32 N p = 0.11 O p = 0.11	C p = 0.09	205	205	C p = 0.43	C p = 0.33 N p = 0.12
193		Fe d = 0.54		204	204	C p = 0.42	C p = 31 N p = 0.12

The selected frontier molecular orbitals involved in the main absorption transition from M06, B3LYP, and PBE0 at 532, 534, and 534 nm of Fe(magneson)$_3$ and 576, 553, and 529 nm of Cr(magneson)$_3$ complexes, respectively, are displayed in Figure 2a and Figure 2b.

One further point of interest in this study is the comparison between the experimental absorbance values and computed oscillator strengths. Experimental absorbance values were scattered in the ranges of 0.073–0.0918, 0.0110–0.0570, and 0.0230–0.0420 for Magneson I, Fe(magneson)$_3$, and Cr(magneson)$_3$ complexes, respectively, depending on the particular spectroscopic determination. Calculated values of the oscillator strength of the transitions in the studied metal complexes were lower than the experimental data. The computed oscillator strengths are found to increase linearly with the number of electrons (N). However, due to several factors, the

experimental values of oscillator strengths are rather scattered with different N. They can be related mainly to the change in interplanar distances in the solvent effects on ε.[24]

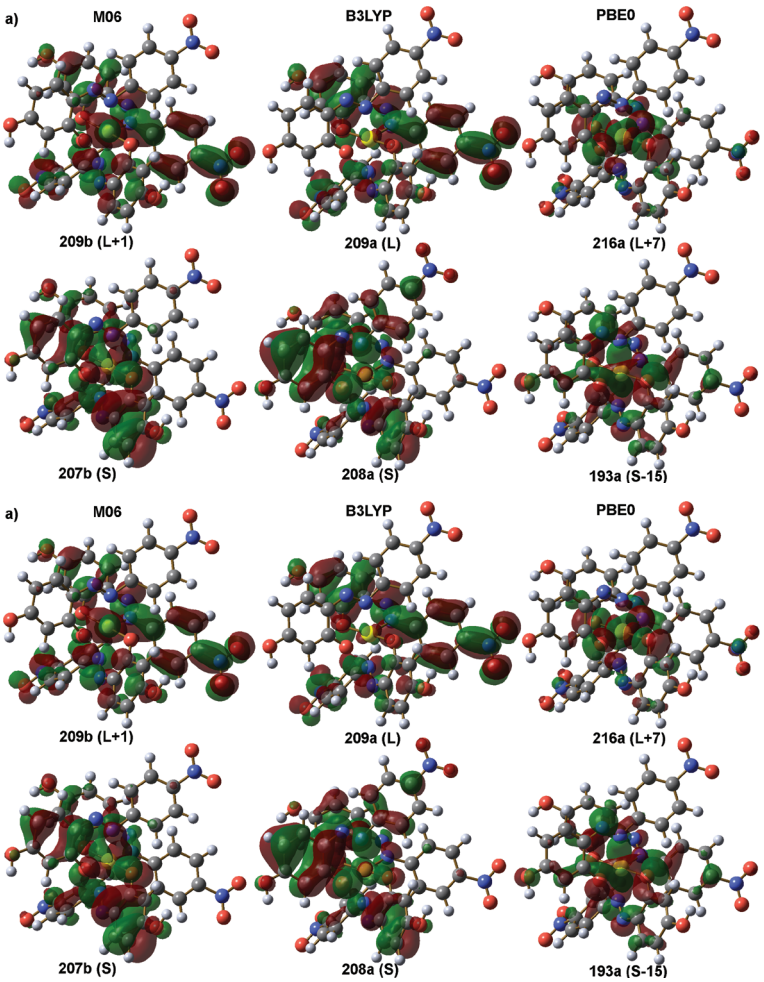

Figure 2. The selected frontier molecular orbitals involved in main absorption transition of a) Fe(magneson)$_3$ and b) Cr(magneson)$_3$ complexes contour isovalue 0.02.

Combining computational studies with experimental spectroscopic results helps us to achieve a deeper understanding of the electronic properties of transition metal complexes. TDDFT calculations show great promise for use in the study of relatively complex electronic absorption spectra of systems that exhibit multiple absorption bands. In this first study of the complexation of the Fe(III) and Cr(III) with Magneson I, TDDFT calculations were carried out to obtain the UV-Vis spectra properties in water. On the basis of the results, the general conclusions are summarized as follows.

The DFT calculations at BP86/TZVP level indicate that the most stable spin states of Fe(III) and Cr(III) complexes are doublet and quartet, respectively. These results are essentially the same as their corresponding literature-known counterparts. The lowest energy structure of both metal complexes is the distorted octahedral geometry. The bond distances and angles are also supported by experimental data in the literature.

The calculated TDDFT results showed that based on M06, B3LYP, and PBE0 functionals, the maximum absorption wavelengths are 446, 459, and 439 nm for Magneson I; 532, 534, and 534 nm for Fe(magneson)$_3$

complex; and 576, 553, and 529 nm for Cr(magneson)$_3$ complex, whereas the experimental results are 450, 534, and 570 nm for Magneson I, Fe(magneson)$_3$, and Cr(magneson)$_3$ complex, respectively. The comparison of the results obtained with each of the exchange-correlation potentials considered here on the Fe(magneson)$_3$ and Cr(magneson)$_3$ complexes allows us to conclude that the M06 and B3LYP functionals are the better choice overall for the TDDFT absorption bands, because of the better matching with the low-lying absorption bands in experimental UV-Vis data. The low-lying absorption bands in UV-Vis spectra were theoretically assigned to LMCT and LLCT for Fe(III) and MLCT, LMCT, and LLCT for Cr(III) complexes. In conclusion, Magneson I can be useful in determining Fe(III) and Cr(III) and the computed results support that the BP86/TZVP level of optimization and M06/TZVP + LANL2TZ or B3LYP/TZVP + LANL2TZ TDDFT approaches are reliable for describing the geometries and spectral properties of open shell ferric and chromic complexes.

Acknowledgments

This work was supported in part by the Scientific and Technological Research Council of Turkey (TÜBİTAK) under grant no: 111T003.

References

1. a) Venkataraman, K.; *The Chemistry of Synthetic Dyes*, vol. III. New York: Academic Press, 1970, b) Beffa, F.; Bock, G. *Metal Complex Dyes for Wool and Nylon-1930 to date. Rev. Prog. Coloration*, 1984.
2. Katz, H. E.; Singer, K. D.; Sohn, J. E.; Dirk, C. W.; King, L. A.; Gordon, H. M. *J Am. Chem. Soc.* **1987**, *109*, 6561–6563.
3. Eich, M.; Wendorff, J. H.; Reck, B.; Ringsdorf, H.; *Makromol. Chem., Rapid Commun.* **1987**, *8*, 59–63.
4. a) Lamansky, S.; Djurovich, P.; Murphy, D.; Abdel-Razzaq, F.; Lee, H. E.; Adachi, C.; Burrows, P. E.; Forrest, S. R.; Thompson, M. E. *J. Am. Chem. Soc.* **2001**, *123*, 4304–4312, b) Nazeeruddin, Md. K.; Humphry-Baker, R.; Berner, D.; Rivier, S.; Zuppiroli, L.; Gräetzel, M. *J. Am. Chem. Soc.* **2003**, *125*, 8790–8797.
5. a) Khatua, S.; Choi, S. H.; Lee, J.; Huh, J. O.; Do, Y.; Churchill, D. G. *Inorg. Chem.* **2009**, *48*, 1799–1801, b) Malins, C.; Glever, H. G.; Keyes, T. E.; Vos, J. G.; Dressick, W. J.; MacCraith, B. D. *Sensors and Actuators B.* **2000**, *67*, 89–95, c) Orellana, G.; Garcia-Fresnadillo, D. *Optical Sensors: Industrial, Environmental and Diagnostic Applications.* Narayanaswamy, R.; Wolfbeis, O. S., Eds.; Springer-Verlag, Berlin Heidelberg, New York, 2004.
6. a) Zollinger, H., *Color Chemistry: Syntheses, Properties, and Applications of Organic Dyes and Pigments*, 3rd Ed.; John Wiley & Sons, USA, 2004, b) Aziz, M. S.; El-Mallah, H. M. *Indian J. Pure Appl. Phys.* **2009**, *47*, 530–534.
7. Beech, W. F.; Drew, H. D. K. *J. Chem. Soc.* **1940**, 608–612.
8. a) Şahin, Ç. A.; Efeçınar, M.; Şatıroğlu, N. *Journal of Hazardous Materials* **2010**, *176*, 672–677, b) Boltz, D. F.; Mellon, M. G. *Analytical Chemistry* **1974**, *46*, 227R–248R, c) Li, J.; Tian, Y.; Huang, Z.; Zhang, X. *Applied Surface Science* **2006**, *252*, 2839–2846.
9. a) Cossi, M.; Scalmani, G.; Rega, N.; Barone, V. *J. Chem. Phys.* **2002**, *117*, 43–54, b) Tomasi, J.; Mennucci, B.; Cammi, R. *Chem. Rev.* **2005**, *105*, 2999–3093.
10. a) Holland, J. P.; Barnard, P. J.; Bayly, S. R.; Dilworth, J. R.; Green, J. C. *Inorg. Chim. Acta* **2009**, *362*, 402–406, b) Tüğsüz, T.; Sevin, F. *Journal of Molecular Structure: THEOCHEM* **2006**, *775*, 29–37, c) Eilmes, A. *Theor. Chem. Acc.* **2010**, *127*, 743–750.

11. Frisch, M. J.; Trucks, G. W.; Schlegel, H. B.; Scuseria, G. E.; Robb, M. A.; Cheeseman, J. R.; Scalmani, G.; Barone, V.; Mennucci, B.; Petersson, G. A.; Nakatsuji, H.; Caricato, M.; Li, X.; Hratchian, H. P.; Izmaylov, A. F.; Bloino, J.; Zheng, G.; Sonnenberg, J. L.; Hada, M.; Ehara, M.; Toyota, K.; Fukuda, R.; Hasegawa, J.; Ishida, M.; Nakajima, T.; Honda, Y.; Kitao, O.; Nakai, H.; Vreven, T.; Montgomery, Jr., J. A.; Peralta, J. E.; Ogliaro, F.; Bearpark, M.; Heyd, J. J.; Brothers, E.; Kudin, K. N.; Staroverov, V. N.; Kobayashi, R.; Normand, J.; Raghavachari, K.; Rendell, A.; Burant, J. C.; Iyengar, S. S.; Tomasi, J.; Cossi, M.; Rega, N.; Millam, J. M.; Klene, M.; Knox, J. E.; Cross, J. B.; Bakken, V.; Adamo, C.; Jaramillo, J.; Gomperts, R.; Stratmann, R. E.; Yazyev, O.; Austin, A. J.; Cammi, R.; Pomelli, C.; Ochterski, J. W.; Martin, R. L.; Morokuma, K.; Zakrzewski, V. G.; Voth, G. A.; Salvador, P.; Dannenberg, J. J.; Dapprich, S.; Daniels, A. D.; Farkas, Ö.; Foresman, J. B.; Ortiz, J. V.; Cioslowski, J.; Fox, D. J. *Gaussian 09, Revision C.1* Gaussian, Inc., Wallingford CT, 2009.
12. Das, P.; Sarmah, P. P.; Borah, M.; Phukan, A. K. *Inorg. Chim. Acta* **2009**, *362*, 5001–5011.
13. a) Tong, Y-P.; Lin, Y-W. *Inorg. Chim. Acta* **2009**, *362*, 2167–2171, b) Yang, Y.; Liu, Z.; Zhong, L.; Qiu, P.; Dong, Q.; Cheng, R.; Vanderbilt, J.; Liu, B. *Organometallics* **2011**, *30*, 5297–5302, c) Thornley, W. A.; Bitterwolf, T. E. *Rev. Roum. Chim.* **2010**, *55*, 765–769.
14. a) Becke, A. D. *Phys. Rev. A* **1988**, *38*, 3098–3100, b) Perdew, J. P. *Phys. Rev. B* **1986**, *33*, 8822–8824.
15. Schaefer, A.; Huber, C.; Ahlrichs, R. *J. Chem. Phys.* **1994**, *100*, 5829–5835.
16. Zhao, Y.; Truhlar, D. G. *Theor. Chem. Acc.* **2008**, *120*, 215–241.
17. a) Becke, A. D. *J. Chem. Phys.* **1993**, *98*, 5648–5652, b) Lee, C.; Yang, W.; Parr, R. G. *Phys. Rev. B* **1988**, *37*, 785–789.
18. Adamo, C.; Barone, V. *J. Chem. Phys.* **1999**, *110*, 6158–6169.
19. a) Hay, P. J.; Wadt, W. R. *J. Chem. Phys.* **1985**, *82*, 299–310, b) Roy, L. E.; Hay, P. J.; Martin, R. L. *J. Chem. Theory Comput.* **2008**, *4*, 1029–1031, c) Ehlers, A. W.; Böhme, M.; Dapprich, S.; Gobbi, A.; Höllwarth, A.; Jonas, V.; Köhler, K. F.; Stegmann, R.; Veldkamp, A.; Frenking, G. *Chem. Phys. Lett.* **1993**, *208*, 111–114, d) Feller, D. *J. Comp. Chem.* **1996**, *17*, 1571–1586, e) Schuchardt, K. L.; Didier, B. T.; Elsethagen, T.; Sun, L.; Gurumoorthi, V.; Chase, J.; Li, J.; Windus, T. L. *J. Chem. Inf. Model.* **2007**, *47*, 1045–1052.
20. a) Stratmann, R. E.; Scuseria, G. E.; Frisch, M. J. *J. Chem. Phys.* **1998**, *109*, 8218–8224, (b) Matsuzawa, N. N.; Ishitani, A. *J. Phys. Chem. A* **2001**, *105*, 4953–4962, (c) Casida, M. E.; Jamorski, C.; Casida, K. C.; Salahub, D. R. *J. Chem. Phys.* **1998**, *108*, 4439–4449.
21. Dixon, D. A.; Shang, M.; Lappin, A. G. *Inorg. Chim. Acta* **1999**, *290*, 197–206.
22. Isaacs, M.; Sykes, A. G.; Ronco, S. *Inorg. Chim. Acta* **2006**, *359*, 3847–3854.
23. Appelt, R.; Vahrenkamp, H. *Inorg. Chim. Acta* **2003**, *350*, 387–398.
24. Connerade, J. P.; Ma, H.; Shen N.; Stavrakas, T. A *J. Phys B: At. Mol. Opt. Phys.* **1988**, *21*, L241–L245.